Measurements of Interbilayer Forces and Protein Adsorption on Uncharged Lipid Bilayers Displaying Poly(ethylene glycol) Chains†

Nadezhda V. Efremova,‡ Bruce Bondurant,§ David F. O′Brien,§,⊥ and Deborah E. Leckband*,‡

Department of Chemical Engineering, University of Illinois, 600 South Mathews Avenue, Urbana, Illinois 61801, and Department of Chemistry, University of Arizona, Tuscon, Arizona 85721

Received September 8, 1999; Revised Manuscript Received December 16, 1999

ABSTRACT: Poly(ethylene glycol) (PEG)-stabilized liposomes were recently shown to exhibit differences in cell uptake that were linked to the liposome charge. To determine the differences and similarities between charged and uncharged PEG-decorated liposomes, we directly measured the forces between two supported, neutral bilayers with terminally grafted PEG chains. The measurements were performed with the surface force apparatus. The force profiles were similar to those measured with negatively charged PEG conjugates of 1,2-distearoyl-*sn*-glycero-3-phosphatidyl ethanolamine (DSPE), except that they lacked the longer ranged electrostatic repulsion observed with the charged compound. Theories for simple polymers describe the forces between end-grafted polymer chains on neutral bilayers. The force measurements were complemented by surface plasmon resonance studies of protein adsorption onto these layers. The lack of electrostatic forces reduced the adsorption of positively charged proteins and enhanced the adsorption of negatively charged ones. The absence of charge also allowed us to determine how membrane charge and the polymer grafting density independently affect protein adsorption on the coated membranes. Such studies suggest the physical basis of the different interactions of charged and uncharged liposomes with proteins and cells.

The properties of tethered polymer chains have been studied extensively from both theoretical and experimental points of view (*1*−*7*). In addition to the fundamental scientific interest in polymer brushes, end-grafted polymers have also been proposed for a wide range of practical applications, such as the stabilization of colloid dispersions, adhesion, and lubrication (*8*−*10*). In recent years, there has been increasing interest in the potential applications of water-soluble polymers in biological systems. In particular, surface modifications of biomaterials and particulate micro-carrier systems used in drug delivery have been studied (*11*, *12*). The brushes of terminally grafted, water-soluble polymer chains are of particular importance for the protection of soft materials, such as liposomes and proteins, from recognition by the cells of the immune system (*13*−*15*).

The current polymer of choice for the majority of these applications is poly(ethylene glycol) (PEG).[1] Its (1) chemical inertness, (2) water solubility (hydrophilicity), (3) low toxicity, (4) insensitivity to changes in solution ionic conditions (due to its nonionic character), and (5) low protein adsorption have made it a particularly suitable polymer for use as a steric stabilizer in such aqueous media as body fluids (*16*−*19*).

Liposomes have long been considered attractive drug carrier and delivery systems because of their large aqueous interior, lipophilic membrane, and biocompatible lipid exterior. However, their use in biomedical applications is limited by their rapid clearance from circulation by the reticuloendothelial system (RES) (*20*). Earlier studies demonstrated that the incorporation of a small amount of lipids with PEG headgroups substantially increases the liposome circulation times (*21*−*23*). This is believed to be due to the steric stabilization of the liposomes by the grafted polymer, which prevents their close approach to cell surfaces.

The majority of the PEG-lipids used so far were anionic (*21*−*24*). Although macrophages do not phagocytize the modified liposomes, the grafted PEG decreases the uptake of the liposomes by carcinoma cells (*25*). This, in turn, decreases the effective delivery of the therapeutic agent. On the other hand, Miller et al. (*25*) demonstrated that neutral and positively charged PEG liposomes are endocytosed more readily by human ovarian carcinoma cells than are anionic PEG liposomes. In addition, macrophages do not efficiently engulf either negatively charged or neutral PEG liposomes. The increased liposome endocytosis of neutral PEG-lipids by carcinoma cells and the simultaneous decrease in phagocytosis by macrophages suggests that the surface charge may

This research was sponsored by Grant Nos. NSF BES 953045, NSF BES 98-10133 (DEL), and NIH GM-40427 (DFO).

* To whom correspondence should be addressed.

Department of Chemical Engineering, University of Illinois at Urbana−Champaign.

Department of Chemistry, University of Arizona.

Department of Biochemistry, University of Arizona.

[1] Abbreviations: BPTI, bovine pancreatic trypsin inhibitor; DPPE, 1,2-dipalmitoyl-*sn*-glycero-3-phosphatidylethanolamine; DSPE, 1,2-distearoyl-*sn*-glycero-3-phosphatidyl ethanolamine; FITC, fluorescein isothiocyanate; FBN, fibrinogen; HSA, human serum albumin; MALDI TOF SIMS, matrix assisted laser desorption time-of-flight surface ion mass spectroscopy; MWC theory, Milner, Witten, and Cates theory; PEG, poly(ethylene glycol); PEG-thiol, *O*-(2-mercaptoethyl)-*O*′-methyl-poly(ethylene glycol); RES, reticuloendothelial system; SAPDS-PEG, 3-stearamidyl-2-(monomethoxyPEG-succinyl)-1-stearoyl-3-aminopropane-1,2-diol; SPR, surface plasmon resonance.

10.1021/bi992095r CCC: $19.00 © 2000 American Chemical Society
Published on Web 03/02/2000

be used to selectively target liposomes to specific cell types.

The physical basis of the stability of PEG-decorated liposomes in vivo, as well as the mechanisms of their interaction with cells, are still not fully understood. This is due, in part, to the complexity of living organisms. Nevertheless, model systems provided important insights into the possible molecular mechanisms underlying the liposome interactions. Using X-ray diffraction, Needham et al. reported that the polymer increases the repulsion both between oriented lipid multilayers and between unoriented multilamelar liposomes (*27*, *28*). Kuhl et al. (*12*, *29*) measured the energy−distance profiles between two negatively charged, PEG-containing supported bilayers. They showed that the Dolan and Edwards (*30*) theory describes the osmotic repulsion between the polymer brushes at low grafting densities. The Alexander−de Gennes model (*5*, *6*) similarly describes the polymer interactions at high grafting densities.

Although these models account for the energy penalty of polymer compression, the PEG coating may also inhibit the nonspecific adsorption of serum proteins, that is, opsonins. This would also prevent the recognition of liposomes by macrophages (*24*, *31*, *32*). The ability of polymer brushes to prevent nonspecific protein adsorption has been addressed theoretically by Jeon et al. (*33*, *34*), Szleifer (*35*), and, more recently, by Halperin (*7*). According to the model of Halperin, the interaction potential between proteins and brush-coated surfaces is given by

$$U_{\mathrm{eff}}(z) \approx U_{\mathrm{bare}}(z) + U_{\mathrm{brush}}(z)$$

Here, z is the altitude of the protein above the surface, $U_{\mathrm{bare}}(z)$ is the interaction potential of the bare adsorbing surface, and $U_{\mathrm{brush}}(z)$ is the interaction potential for the polymer brush. Although the repulsion by grafted chains may be due to the inability of the proteins to compress the polymer (*33*, *34*), above a certain grafting density, proteins can diffuse through the polymer brush and adsorb (*7*, *35*). Halperin predicted the grafting densities at which the proteins would preferentially (i) diffuse to the underlying substrate and adsorb (primary adsorption), (ii) adsorb at the outer surface of the brush (secondary adsorption), or (iii) compress the polymer film (*7*, *35*).

In this paper, we used surface plasmon resonance and direct force measurements to identify the liposome properties that could lead to differences in opsonization and cell uptake of various polymer−lipid formulations. The neutral PEG-lipids allowed us to test models for the interactions of membrane surfaces bearing terminally grafted PEG both with other PEG films and with soluble proteins. With the surface force apparatus (SFA), we directly measured the interactions between terminally grafted polymer layers at different chain densities. The force−distance curves qualitatively agreed with scaling theory predictions and with previous measurements. The force measurements were complemented by surface plasmon resonance studies of protein adsorption onto both neutral and negatively charged polymer layers. The results show that protein adsorption is blocked at the chain density that is predicted to prevent diffusion through the brush. These studies show how the surface charge and the polymer grafting density influence the adsorption of different proteins.

MATERIALS AND METHODS

Materials. High-purity 1,2-dipalmitoyl-*sn*-glycero-3-phosphatidylethanolamine (DPPE), 1,2-distearoyl-*sn*-glycero-3-phosphatidylethanolamine (DSPE), and DSPE-PEG_{2000} were purchased in powdered form from Avanti Polar Lipids, Inc. All of the salts were high purity (>99.5%) and were purchased from Aldrich. Water was purified with a Milli-Q UV filtration system (Millipore), with a resistivity of 18.2 MΩ. HPLC-grade methanol and chloroform were from Mallinckrodt. Monomethoxy PEG_{2000} with a $M_w/M_n = 1.02$ (determined by matrix assisted laser desorption time-of-flight surface ion mass spectroscopy (MALDI TOF SIMS)), stearic acid 99%, and *rac*-3-aminopropane-1,2-diol were purchased from Aldrich and used without further purification. FITC-DSPE was from Molecular probes. Gold (99.99%) and silver shot (99.99%) for the evaporation of metal films were purchased from Aldrich. Chromium chips (99.997%) for the evaporation of adhesion layers between gold and glass were purchased from Alfa Aesar.

Synthesis of 3-Stearamidyl-2-(monomethoxyPEG-succinyl)-1-stearoyl-3-aminopropane-1,2-diol (SAPDS-PEG). 1. PEG Succinate. Monomethoxy PEG_{2000} (9 g, 4.5 mmol) was acylated with succinic anhydride (2.24 g, 22.4 mmol) and dry pyridine (2.2 g, 28 mmol) in dry, alcohol-free chloroform, under argon, at reflux, for 4 h. Evaporation of the reaction mixture with *p*-xylene (40 mL) provided crude product (11.3 g) ($R_f = 0.29$) in 10% methanol and 90% chloroform on normal silica gel. The product was purified by recrystallization from 5/1 tetrahydrofuran/diethyl ether (100 mL) followed by silica gel column chromatography with an elution gradient from 100% chloroform to 15% methanol, 85% chloroform. Pure PEG-succinate (6 g, 64% yield) was recovered. ^{1}H NMR ($CDCl_3$): 4.26−4.23 (t, $J = 3.2$ Hz, 2H, $-CH_2O(CO)-$), 3.87−3.84 (t, $J = 4.7$ Hz, 2H, $-CH_2CH_2O(CO)-$), 3.75−3.36 (m, 180 H, $(OCH_2CH_2)_n$), 3.54 (s, 3H, OCH_3), 2.66−2.58 (m, 4H, $-O_2CCH_2CH_2COOH$) ppm. FTIR (KBr): 2930−2740 cm^{-1} (broad), 1734 (sharp) cm^{-1}.

2. rac-Boc-3-aminopropane-1,2-diol. Di-*tert*-butyl dicarbonate (2.6 g, 12 mmol), 3-aminopropane-1,2-diol (1.0 g, 11 mmol), and triethylamine (1.2 g, 6 mmol) were added to 10 mL of dry dichloromethane. The reaction mixture was stirred at room temperature under argon for 18 h. TLC in 15% methanol, 1% H_2O, and 84% chloroform yielded the product with $R_f = 0.8$, which stained with iodine as well as with ninhydrin in acetic acid upon prolonged heating. Purification by column chromatography, using 10% methanol, 0.5% water, and 89.5% chloroform as eluent, on normal-phase silica gel produced pure Boc-3-aminopropane-1,2-diol in 40% yield (800 mg). ^{1}H NMR ($CDCl_3$): 5.0 (broad s, 1H, NH), 3.76−3.68 (m, 1H, HCOH), 3.62−3.44 (m, 2H, $-CH_2OH$), 3.30−3.17 (m, 2H, $-CH_2N-$), 2.8 (broad s, 2H, $-CH_2OH$ and $-CHOH$), 1.42 (s, 9H, $C(CH_3)_3$) ppm. FTIR ($CHCl_3$/NaCl): 3353 cm^{-1} (broad, strong), 1690 cm^{-1} (sharp, strong). FABMS: calculated MW 191.2, found *m*/*z* 192.1.

3. rac-Boc-3-aminopropane-1,2-distearate. rac-Boc-3-aminopropane-1,2-diol (0.3 g, 1.6 mmol) and pyridine (0.496 g, 6.28 mmol) were combined in dichloromethane and cooled to 0 °C under argon. Stearoyl chloride (1.423 g, 4.71 mmol) in 14 mL of benzene was added to the solution. The stearoyl chloride was previously prepared from stearic acid by

treatment with oxaloyl chloride. The reaction mixture was allowed to reach 25 °C and stirred for 14 h under argon. Methanol (10 mL) was added, and the solvent was removed under reduced pressure. The resulting viscous oil was dissolved in diethyl ether (50 mL) and filtered. The precipitate was washed with 2 × 10 mL of diethyl ether. The combined ether solution was extracted with the following: 2% aq HCl (50 mL), deionized water (2 × 25 mL), 5% aq Na_2CO_3 (4 × 25 mL), deionized water (3 × 50 mL), and saturated brine (3 × 10 mL). The organic phase was dried over sodium sulfate, and the solvent was removed under reduced pressure to yield 1.97 g of crude product. Purification by column chromatography with combined chloroform/hexanes produced 1.0 g (88% yield) of purified Boc-distearoylAPD. ^{1}H NMR: ($CDCl_3$): 5.14−5.05 (q, J = 5.7 Hz, 1H, NH), 4.8−4.7 (m, 1H, HCO(CO)R), 4.30−4.23 (dd, J = 12, 4.2 Hz, 1H, $-CH_2O(CO)R$), 4.15−4.09 (dd, J = 12, 5.7 Hz, 1H, $CH_2O(CO)R$), 3.49 (s, 1.4H, water), 3.42−3.28 (m, 2H, $-CH_2N-$), 2.35−2.28 (t, J = 7.8 Hz, 4H, $-CH_2COO-$), 1.68−1.54 (m, 4H, $-CH_2CH_2COO-$), 1.44 (s, 9H, $-C(CH_3)_3$) 1.32−1.19 (m 56H, $(CH_2)_{14}$), 0.9−0.86 (t, J = 6.9 Hz, 6H, $-CH_2CH_3$) ppm.

4. 3-Stearamidyl-1-stearoyl-3-aminopropane-1,2-diol. A 1:1 (v/v) mixture of trifluoroacetic acid and dichloromethane (10 mL) was cooled to −10 °C in a dry ice−brine bath. Boc-distearoylAPD (500 mg, 0.69 mmol) was added, and the reaction was stirred vigorously for 20 min, at which time the reaction was found to be complete by TLC analysis. Toluene (20 mL) was added, and the dichloromethane and TFA were removed under reduced pressure without raising the temperature. Upon the formation of a copious white precipitate, the evaporation was continued at 25 °C until all of the solvent was gone. The white powder (342 mg) was further purified by normal-phase HPLC on a Waters μPorasil column (40 × 200 mm) that was prewashed with 2% triethylamine in methanol (200 mL) followed by chloroform (800 mL). Elution of the product mixture was done with a gradient from pure chloroform to 5% (v/v) methanol in chloroform. The product (R_f = 0.8 in 5% methanol, 95% chloroform) was obtained in 66% yield (285 mg). A rearrangement from a possible 1,2-disubstituted APD to a 1,3-disubstituted APD either occurred during work up or during purification. This acyl-chain shift is demonstrated by a difference of 0.14 ppm in the α-protons of two stearoyl groups. ^{1}H NMR: 6.0−5.85 (m, 1H, NH), 5.78−5.70 (m, 0.3H, NH), 4.78−4.85 (m, 0.3H, HCO(CO)−R), 4.20−4.10 (q, J = 5.1 Hz, 1H, $CH_2O(CO)R$), 4.06−3.96 (q, J = 7.5 Hz, 1H, $H_2CO(CO)R$), 3.94−3.84 (m, 1H, HCOH), 3.6−3.4 (m, 2H, $-CH_2N-$ and HCOH), 3.3−3.2 (m 1H, $-CH_2N-$), 2.38−2.28 (t, J = 7.5 Hz, 2H, $-CH_2COO-$), 2.25−2.15 (t, J = 7.8 Hz, 2H, $-CH_2(CO)N-$), 1.7−1.5 (m, 14H, $-CH_2CH_2COO-$ and water) 1.4−1.1 (m, 60H, $(CH_2)_{14}$ and $(CH_2)_{15}$), 0.90−0.80 (t, J = 6.8 Hz, 6H, $-CH_2CH_3$) ppm. FABMS: calcd for $C_{39}H_{77}NO_4$ 623.59, found 624.59.

5. 3-Stearamidyl-2-(monomethoxyPEG-succinyl)-1-stearoyl-3-aminopropane-1,2-diol (SAPDS-PEG). PEG-succinate (230 mg, 0.1 mmol) and HOBT (41 mg, 0.3 mmol) were azeotropically dried with benzene (2 × 50 mL) and combined with EDC (76 mg, 0.4 mmol) and 3-stearamidyl-1-stearoyl-3-aminopropane-1,2-diol (50 mg, 0.08 mmol) in dry, alcohol-free chloroform (2 mL). The reaction was then stirred under argon for 8 h, followed by the addition of triethylamine (0.6 mmol). The reaction was then allowed to stir for 3 h, after which the solution was combined with *p*-xylene (5 mL), and the solvent was removed under reduced pressure. The resulting solid was precipitated three times from ethanol to afford 220 mg of crude product. This solid was purified by normal-phase HPLC on silica with a gradient from 100% chloroform to 10% methanol, 90% chloroform. The sample was further purified by reversed-phase (C18 column 40 × 100 mm) elution with 20% water and 80% acetonitrile, followed by 50% methanol and 50% 2-propanol to give 18 mg (9% yield) of pure PEG-APD lipid. ^{1}H NMR in $CDCl_3$: 6.15−6.05 (m, 1H, NH), 5.15−5.05 (m, 1H, HCO(CO)R), 4.3−4.2 (m, 3H, $-CH_2O(CO)R$), 4.1−4.0 (m, 1H, $-CH_2O-(CO)R$), 3.9−3.8 (t, J = 4 Hz, 2H, $-OCH_2CH_2O(CO)R$), 3.8−3.3 (m,180 H $CH_3O(CH_2CH_2O)_n$), 2.8−2.5 (m, 4H, $-O(CO)CH_2CH_2COO-$), 2.32−2.22 (t, J = 7.5 Hz, 2H, $-CH_2COO-$), 2.2−2.1 (t, J = 7.6 Hz, 2H, $-CH_2(CO)N-$, 1.5−1.7 (m, 42H, CH_2CH_2COO- and water), 1.1−1.4 (m, 58H, $(CH_2)_{14}$ and $(CH_2)_{15}$), 0.09−0.08 (t, J = 7.2 Hz, 6H, $-CH_2CH_3$) ppm. FABMS: envelope centered at m/z = 2500.8 with peak spacing of 44.

Monolayers at the Vapor−Water Interface. Solutions of PEG-lipid (SAPDS-PEG) and pure DSPE were prepared in 9:1 chloroform/methanol solutions. Mixtures of 1.3, 4.5, and 10.0 mol % SAPDS-PEG in a matrix of DSPE were prepared by mixing solutions of the pure compounds in the appropriate proportions. Measurements of surface pressure versus area were made with a commercial Langmuir−Blodgett trough (NIMA, type 611), equipped with a Wilhelmy balance.

Preparation of Supported Lipid Bilayers Displaying Grafted PEG. The grafted polymer layers (Figure 1) were prepared by Langmuir−Blodgett deposition of the mixed lipid monolayers either onto hydrophobized mica or onto hydrophobized gold films on glass. The monolayers comprised DSPE and SAPDS-PEG in the proportions stated above. After the lipids were spread on the water surface, they were compressed to an average area of 43 Å^2 per lipid. The monolayer was then deposited at a constant pressure of

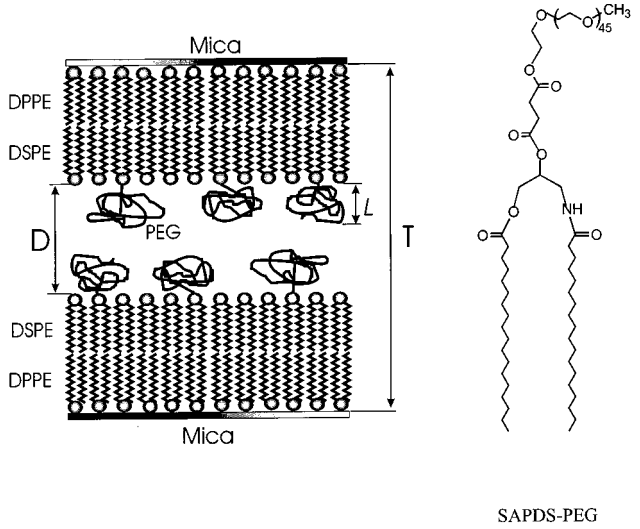

FIGURE 1: Schematic representation of the two opposing bilayer-coated mica surfaces used in direct force measurements. The bilayer contact defines $D = 0$. L is the equilibrium thickness of the polymer layer. The structure of the SAPDS-PEG is shown to the right of the illustrated sample configuration.

42 mN/m onto a hydrophobic, crystalline monolayer of DPPE on mica, prepared by Langmuir−Blodgett deposition (*12*). Adjusting the SAPDS-PEG mole fraction in the monolayer controlled the polymer grafting density. The transfer ratio—that is, the area transferred relative to the area coated by the film—was close to unity in all cases.

Force Measurements. Force measurements were conducted with the Mark II surface force apparatus (*36*) in a temperature-controlled room at 25 °C. The forces were measured between two bilayer-coated mica sheets (see Figure 1) that were back-silvered and glued onto cylindrical silica disks. The distance between the bilayer surfaces was determined with a resolution of ±1 Å by multiple-beam interferometry (*26*). The force between the bilayer surfaces was measured with the resolution of 10^{-4} mN from the deflection of a variable cantilever spring that supported the lower disk. The chamber of the instrument that houses the samples was filled with a 10 mM sodium phosphate buffer solution (pH 7.0) containing 30 mM KNO_3. The solution was saturated with DSPE to prevent desorption of the lipid bilayers during the measurements. The solution was prefiltered twice through a surfactant-free 0.2 μm Durapore membrane (Millipore).

Surface Plasmon Resonance (SPR) Measurements. SPR measurements were carried out with a home-built, computer-controlled setup based on the Kretchman configuration (*37, 38*). A flow cell with a volume of 0.4 mL was used to measure the equilibrium protein adsorption. This volume was large enough so that we could disregard any depletion of bulk protein solution due to adsorption. A system of three-way valves allowed us to inject or change solutions without introducing air into the cell. The injection rate was controlled with a syringe pump (KD Scientific) and was 12−13 mL/h for all studies. To remove protein aggregates, the protein solutions were centrifuged for 10 min at 14 000 rpm immediately prior to use.

The samples that were used for SPR experiments consisted of several stacked films. The glass slides were thoroughly cleaned with a mixture of concentrated hydrochloric acid, hydrogen peroxide, and water (1:1:1, volume ratio) at 60 °C. The dried slides were then coated with a 20 Å chromium adhesion layer and a 480−500 Å gold overlayer, by the resistive evaporation of these metals in a vacuum. The gold-coated substrates were immersed in a 1 mM solution of 1-octadecanethiol (Aldrich, 98%) in ethanol, immediately after the metal evaporation, and left overnight. The slides were then rinsed with ethanol and dried with filtered nitrogen. The advancing water contact angles were measured with a Gaertner goniometer−microscope and were 110 ± 3°. The mixed lipid monolayers were then deposited on these slides as described above.

For each of the SPR samples, we measured the dependence of the reflected beam intensity, I_r, on the incident angle Θ before and after the deposition of the overlayers. The obtained I_r versus Θ profiles were fitted to theoretical dispersion curves, which were calculated using Fresnel reflectivity coefficients for a multilayer system (*39*). Provided that the refractive index, n, of the sample material in the dry state is known, this simulation allows us to determine a calibration slope, k, that relates the changes in the resonance angle, Θ_r, to the changes in the effective optical thickness, d, of the sample layer, $\Delta d = k\Theta_r$. In addition, for a known specific gravity, ρ, of the adsorbing/desorbing material, the changes in the effective optical thickness can be readily converted into the surface density, $\Gamma = \rho\Delta d$. We assumed the specific gravities of adsorbed protein layers to be the same as in the solid state. The reported values of the crystalline proteins are 0.94 g/cm^3 for FBN (*40*), 0.98 g/cm^3 for BPTI (*41*), and 1.024 g/cm^3 for HSA (*42*). It should be noted that, in this calculation, Δd accounts for incomplete monolayer coverages, so that there are no further assumptions regarding the structure of protein monolayers.

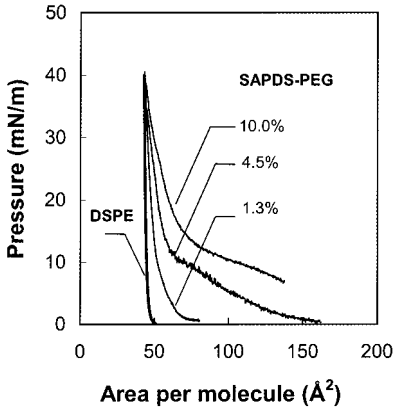

FIGURE 2: Monolayer compression isotherms of DSPE and mixed DSPE/SAPDS-PEG (1.3, 4.5, and 10 mol % SAPDS-PEG) at 21 °C. The average area per molecule in all indicated films is 43 Å^2 at 42 mN/m.

The estimated accuracy of the SPR measurements was ±0.02 mg cm^{-2}. It should be noted that the total thickness of all of the layers on the surface of a gold metal film was always less than 800 Å. At these distances, the instrumental output parameter, Θ_r, varies linearly with the surface density of the material present at the solid liquid interface (*43, 44*).

Fluorescence Imaging of the Supported Lipid Bilayers Displaying Grafted PEG. Fluorescence microscopy was used to test the lateral miscibility of the PEG-lipid with DSPE. To visualize the layer structure, 1 mol % of FITC-labeled DPPE was added to the DSPE/SAPDS-PEG and DSPE/DSPE-PEG monolayers. The monolayers were deposited onto freshly cleaved hydrophobized mica sheets and transferred under water into a cell used for fluorescence microscopy. The cell was filled with buffer solution (40 mM PBS, pH 7.0). Fluorescence micrographs were acquired with an Olympus BX-60 microscope equipped with an 80× objective (the total magnification of microscope was 1400×), a mercury arc-light source, a set of filters, and a CCD camera (Photometrics, 512 × 512 pixels, liquid nitrogen cooled). The CCD camera was connected to a PC and controlled via PMIS software (Photometrics).

RESULTS AND DISCUSSION

Monolayers at the Vapor−Water Interface. Figure 2 shows the pressure−area curves of mixed DSPE/SAPDS-PEG monolayers containing different mole percentages of the PEG-lipid. As the concentration of SAPDS-PEG in the monolayer increases, the lateral pressure at a given area per molecule increases correspondingly. This additional surface pressure is evidently due to the lateral interactions between PEG chains at the vapor−water interface. At large molecular areas, the PEG chains are concentrated at the water surface (*45, 46*).

Table 1: Parameters of Polymer Layer as a Function of SAPDS-PEG Grafting Density

% of SAPDS-PEG (mol %)	packing area[a] per molecule (Å)	packing area[a] per PEG chain σ (Å^2)	distance between grafting sites s (Å)	PEG chain extension[b] (L (Å))
		mushroom		
1.3	43	3300	65	42 ± 5
		weak overlap		
4.5	43	960	35	42 ± 5
		brush		
10	43	430	23	60−65

[a] Determined from monolayer compression isotherms (Figure 2). [b] Determined from range of forces in Figure 4.

At surface pressures near the inflection point, at ~10 mN/m, the compressed polymer chains can no longer remain at the interface and extend into the water subphase (*12*, *47*). The transition pressure is similar to that measured with pure PEG polymer chains adsorbed at the vapor−water interface (*48*).

The mean area per molecule at all four SAPDS-PEG concentrations at a surface pressure of 42 mN/m is 43 Å^2 (Figure 2). With this information, and the mole fraction of SAPDS-PEG in the monolayers, we determined the mean area per PEG chain. For 1.3 mol %, it was 3300 Å^2, which corresponds with the nonoverlapping "mushroom" regime. With 4.5 mol % and 10 mol % SAPDS-PEG, the area per chain was 960 and 430 Å^2, respectively. As previously reported, these values correspond to weakly overlapping chains and to polymer brushes, respectively. Table 1 summarizes the packing densities and the distances between grafting sites for each of the SAPDS-PEG concentrations used.

Fluorescence Microscopy of Supported PEG-Lipid Bilayers. To check whether the PEG-lipid mixes laterally with the DSPE, we carried out a fluorescent microscopy study of the supported bilayers on mica. In the control experiments, it was verified that FITC-labeled DPPE is homogeneously distributed in DSPE monolayers. In all the cases investigated (1.3, 4.5, and 10.0 mol % SAPDS-PEG), the monolayers were structureless on a micron scale, and there was no evidence for demixing. A representative fluorescence image of the monolayer containing 10.0 mol % SAPDS-PEG is shown in Figure 3A. By contrast, Figure 3B shows a supported monolayer containing DSPE and the negatively charged DSPE-PEG at 10.0 mol %. In the latter case, the grainy structure of the monolayer indicates that the two components are not completely miscible. Thus, in supported bilayers, the SAPDS-PEG appears to exhibit better miscibility with DSPE than DSPE-PEG does.

Force Measurements of Lipid Bilayer Interactions. Definition of Zero Separation, $D = 0$ Å. We define $D = 0$ Å as the point of contact between the opposed, nominally dehydrated lipid bilayer surfaces (*50*). The difference in the distance of closest intersurface approach before and after removal of the organic layers from the mica defines the total thickness, T, of both bilayers together with the polymer headgroups (see Figure 1). The combined thickness of two compressed PEG layers is then determined by subtraction of the thicknesses of the two bilayers from the total thickness (*12*). Thus,

$$t_{PEG} = (T - 2(t_{DSPE} + t_{DPPE}))/2$$

For these determinations, we used the reported values of 28 and 27 Å for the respective thicknesses of the DSPE and DPPE monolayers (*50*).

Force Measurements between Grafted PEG Chains. The force versus distance profiles between the opposing lipid monolayers containing 1.3, 4.5, and 10.0 mol % of SAPDS-PEG are summarized in Figure 4. In the absence of grafted polymer, neutral DSPE layers adhere due to the attractive van der Waals force between them (*50*). The DSPE monolayers containing bound PEG were, however, repelled at all separations by the osmotic repulsion between the polymer chains (cf. Figure 4). The force between 1.3 mol % ("mushroom" regime) and 4.5 mol % ("weak overlap") SAPDS-PEG monolayers extends up to $\sim 2 \times 42 \pm 5 \approx 84$ Å. This is roughly the separation at which the chains begin to interact. It is also comparable with twice the 35 Å Flory radius of 2000 MW poly(ethylene oxide). At 10 mol %, the steric repulsion between the two dense brushes begins at $2 \times 62 \pm 3$ Å (Figure 4). This is expected because of the more extended conformation of the polymer chains.

It should be noted that for each of the PEG grafting densities investigated here, the force−distance dependence was always fully reversible and did not exhibit hysteresis between the advancing−receding branches of the curve. This indicates that the measured forces reflect the equilibrium values at each separation.

The ranges of the steric force are consistent with those reported for the bilayers containing negatively charged DSPE-PEG (*12*). Namely, the brush thickness was 65−75 Å, and the film thicknesses were 35 and 50 Å for the 1.3 and 4.5 mol % films, respectively.

Comparison of Measured Force−Distance Profiles with Polymer Theories. In this paper, we compared the forces between 4.5% and 10.0% brushes (i) with the Alexander−de Gennes model (*5*, *6*) and (ii) with the Milner, Witten, and Cates (MWC) mean field calculation for the interaction free energy between surfaces coated with end-grafted chains in good solvent (*4*). The Dolan and Edwards model was used to fit the force curves obtained with dilute polymer chains (*30*).

Alexander−de Gennes theory predicts the following force versus distance dependence for two compressed polymer brushes attached to crossed cylindrical surfaces of geometric average radius R (*29*)

$$\frac{F(D)}{R} \approx \frac{16KT\pi L}{35s^3}\left[7\left(\frac{2L}{D}\right)^{5/4} + \left(\frac{D}{2L}\right)^{7/4} - 12\right] \qquad (1)$$

if $D \ll R$, $D < 2L$.

It should be noted that eq 1, does not give the exact value for the numerical prefactor. The equilibrium brush thickness is given by $L = s(R_F/s)^{5/3}$ where $s = 2(\sigma/\pi)^{1/2}$ is the average distance between the grafting points on the surface, and σ is the area per polymer chain. In our case the latter is controlled by the monolayer composition (see Table 1).

Figure 5 shows the fits of eq 1 to the experimental force−distance profiles obtained with 4.5 mol % and 10 mol %

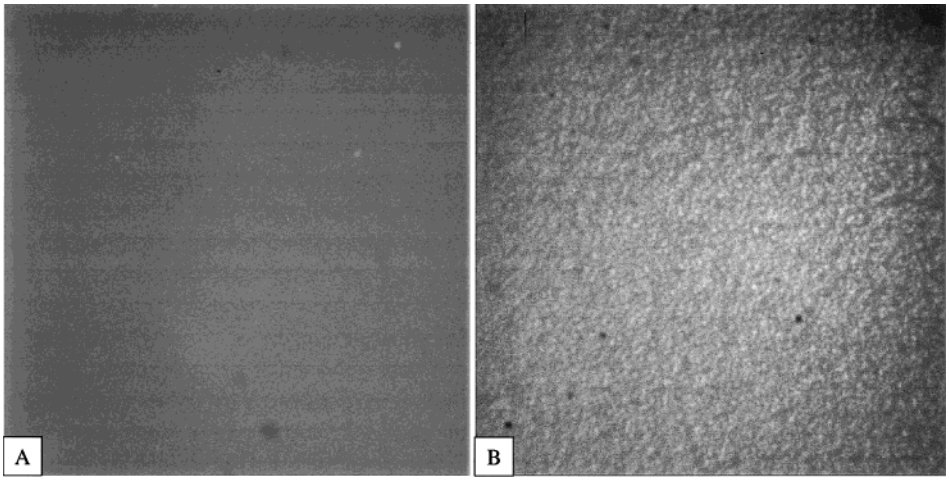

FIGURE 3: Fluorescent micrographs (1400× magnification) of supported lipid DSPE monolayers containing (A) 10 mol % SAPDS-PEG and (B) 10 mol % DSPE-PEG. The monolayers were prepared by Langmuir−Blodgett deposition of the indicated monolayers on a crystalline monolayer of DPPE supported on mica. The films contained 1 mol % of the fluorescent dye FITC-DSPE.

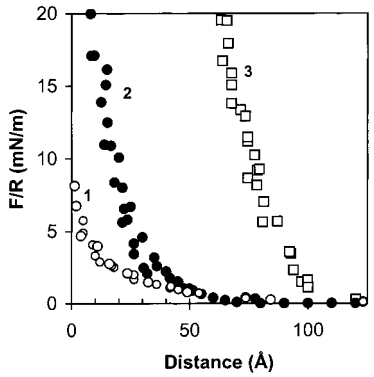

FIGURE 4: Force vs distance profiles between PEG films at different polymer grafting densities. The interacting monolayers contained DSPE and the following molar concentrations of SAPDS-PEG: 1.3 mol % (open circles), 4.5 mol % (filled circles), and 10.0 mol % (open squares). Measurements were carried out at pH 7.0 and 25 °C. The bathing solution contained 10 mM phosphate and 30 mM KNO_3.

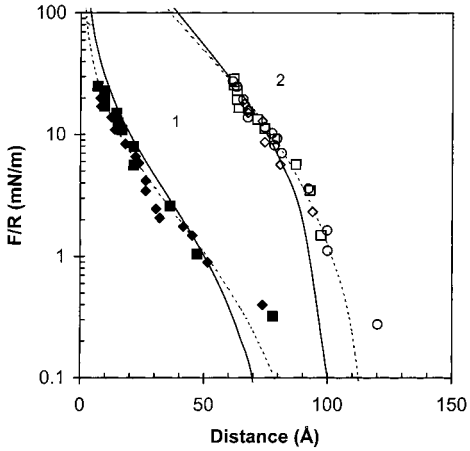

FIGURE 5: Force vs distance profiles between monolayers containing 4.5 mol % (1) and 10.0 mol % (2) SAPDS-PEG. The solid lines show fits of the data to the Alexander−de Gennes model, and the dashed lines indicate the fit of the MWC theory to the data. The fitted parameters are given in Table 2 and in the text.

SAPDS-PEG monolayers. Both the brush thickness and the numerical prefactor were allowed to vary. With 10 mol % PEG-lipid films, the fit gave a brush thickness of 52 ± 3 Å. This is less than the 62 ± 3 Å range of the steric repulsion

Table 2: Fitted Parameters for DSPE/SAPDS-PEG Force Profiles

% of SAPDS-PEG (mol %)	theoretical equation	prefactor *A*	fitted theoretical thickness *L* (Å)	standard deviation (mN/m)
1.3%, L_{exp} = 42 Å	Dolan−Edwards, eq 3	0.163 ± 0.008	29 ± 1	1.08
4.5%, L_{exp} = 42 Å	Alexander−de Gennes, eq 1	0.63 ± 0.03	40 ± 2	4.34
	MWC, eq 2	3.7 ± 0.2	52 ± 3	1.89
10.0%, L_{exp} = 62 ± 3 Å	Alexander−de Gennes, eq 1	3.6 ± 0.2	52 ± 3	3.32
	MWC, eq 2	0.45 ± 0.02	62 ± 3	3.09

(see Table 2). Figure 5 suggests that the Alexander−de Gennes fit to the force profile decreases too rapidly at large separations and, thus, underestimates the tail portion of the data obtained with these short polymer chains. With 4.5% PEG-lipid, the theoretical fit yielded a polymer layer thickness of 40 ± 2 Å, which agrees with the experimentally measured thickness of 42 ± 3Å. The Alexander−de Gennes model also underpredicts the tail of the force profile at the lower polymer density. The results are summarized in Table 2.

Both of these values are in good agreement with previous work: namely, the reported fitted values were 34 Å for weakly overlapping chains and 54 Å for the brush (*12*). The values of the prefactor determined earlier (*12*), 1.65 (4.5%) and 1.83 (10%), differ from our values of 0.63 ± 0.03 and 3.6 ± 0.2 (see Table 2). The overall shape and range of the forces are nevertheless very similar. These differences may be due, in part, to the indirect determination of the steric forces by subtraction of the electrostatic force from the net force profile (*12, 29*). The differences in the miscibility of DSPE-PEG and SAPDS-PEG with DSPE may also contribute to the difference.

In contrast to the Alexander−de Gennes model (*5, 6*), which assumed a step function for the segment density profile, the mean field analysis of Milner, Witten, and Cates (MWC) (*4*) predicted a parabolic segment profile for brushes. The MWC theory was used by Kenwothy et al. to express the distance dependence of the pressure *P* between bilayers exposing grafted PEG chains (*51*). We have similarly used this expression to estimate the repulsive force between two crossed cylinders bearing terminally grafted chains as a

function of their separation. The corresponding equation is (*52*)

$$\frac{F(D)}{R} = 2\pi E(D) = 2\pi \int P(D)dD = -4\pi P_o\left[\frac{2L_o}{D} + \left(\frac{D}{2L_o}\right)^2 + \frac{1}{5}\left(\frac{D}{2L_o}\right)^5 - \frac{9}{5}\right] \quad (2)$$

where

$$P_o = \frac{kTN}{2}\left(\frac{\pi^2}{12}\right)^{1/3}\frac{a^{4/3}}{s^{10/3}}$$

Here, N is the number of segments in a polymer chain and a is the length of a segment. The equilibrium noncompressed brush thickness in this case is given by

$$L_o = \left(\frac{12}{\pi^2}\right)^{1/3}\frac{Na^{5/3}}{s^{2/3}}$$

There is a simple correlation between the equilibrium brush thickness in the MWC theory, L_o, and the equilibrium brush thickness in the Alexander−de Gennes model, L: namely, $L_o = 1.3L$. It should be noted that eq 2 was derived for two interacting impenetrable polymer brushes and not for a polymer brush confined by a hard wall.

The fits of eq 2 to the experimental force−distance profiles for weakly overlapping chains (4.5 mol % SAPDS-PEG) and for brushes (10 mol % SAPDS-PEG) are shown in Figure 5 (dotted lines). In this case, both the brush thickness and the numerical prefactor were allowed to vary. The MWC theory (eq 2) appears to describe the experimental data better than the Alexander−de Gennes model at large separations. For the 4.5 mol % PEG-lipid, the fitted polymer layer thickness was 52 ± 3 Å. With 10 mol % PEG-lipid, the fitted brush thickness was 62 ± 3 Å. Both measurements are in good agreement with the measured thicknesses of these neutral PEG monolayers (Table 2). Our finding that the parabolic profile describes the segment distribution within the brush better than the step function agrees with results from neutron reflectivity studies of mixed DSPE-PEG/DSPE monolayers (*46, 53, 54*).

To fit the experimental force profiles for the "mushroom" regime, we used Dolan and Edwards' theory for interactions between dilute mushrooms (*30*). The Dolan and Edwards equation for the force as a function of distance is approximated by

$$F(D)/R \approx (72\pi kT/\sigma)e^{-D/R_g} \quad (3)$$

where R_g is the radius of gyration of a random coil in a θ solvent. This gives the thickness of the polymer layer normal to the bilayer surface. Because water is a good solvent for PEG at 25 °C, R_g in eq 3 can be substituted by the Flory radius, R_F.

Figure 6 displays the fit of the experimental data for 1.3 mol % SAPDS-PEG to the above equation. Again, both the numerical prefactor and R_F were allowed to vary. As one can see, the fit was remarkably good. The variable parameters are listed in Table 2. The theoretical fit yielded a decay length $R_F = 29 \pm 1$ Å. This is close to the 35 Å Flory radius of PEG 2000 and agrees with previous measurements (*12*).

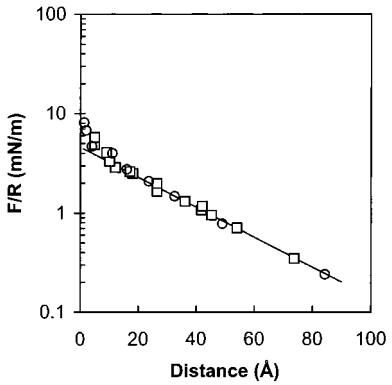

FIGURE 6: Fits of the force between membranes containing 1.3 mol % SAPDS-PEG monolayers to the Dolan and Edwards equation (eq 3). The fitted decay length was $R_g = 29 \pm 1$ Å, and the prefactor was 0.16 ± 0.01 mN/m.

Protein Adsorption Studies. The previous studies indicated that PEG behavior is described by theories for simple chains. We sought to also determine whether simple theories could describe protein interactions with polymer-coated surfaces. To investigate the adsorption of protein onto the PEG films, we used three proteins, namely: human serum albumin (HSA), human fibrinogen (FBN), and bovine pancreatic trypsin inhibitor (BPTI). We compared the data obtained with these three proteins with a recently developed model (*7*), which describes the adsorption of proteins onto surfaces with grafted chains in a good solvent. The three chosen proteins differ significantly in shape, size, and charge. BPTI is a very small (21 × 21 × 30 Å) globular protein, MW 6000, with a p*I* of 10.5 (57, 58). Fibrinogen is a large (55 × 55 × 460 Å) rodlike protein of MW 340 000, with a p*I* of 5.5 (55). Finally, HSA has the dimensions 38 × 38 × 150 Å. Its molecular weight and p*I* are 66 200 and 4.7, respectively (59).

The adsorption of proteins onto DSPE monolayers containing 0, 1.3, 4.5, and 10 mol % of SAPDS-PEG and 1.3 and 4.5 mol % of DSPE-PEG was measured in situ using the SPR technique. The DSPE-PEG monolayers were only studied at two PEG-lipid concentrations. This was on account of the fluorescence data, which indicate that the mixed DSPE-PEG monolayers are slightly inhomogeneous at higher polymer densities. In our experiments, the cell housing the sample was first preequilibrated with 10 mM phosphate buffer (pH 7.0) containing 30 mM $NaNO_3$. The same buffer was used to prepare protein solutions with concentrations ranging from 0.1 to 2 mg/mL. The adsorption was initiated by the injection of the solution into the flow cell. After the protein adsorption saturated, the solution was rinsed from the cell with buffer, and the amount of protein remaining was determined.

Figure 7 shows a characteristic adsorption time course. The adsorption saturated within 20 min. The apparent desorption observed upon flushing the cell is due, in part, to changes in the refractive index of the bulk solution (*60*). A slight decrease in the amount of the bound material may also contribute to this effect. After approximately 10 min of rinsing, the effective optical thickness stabilized, and the amount of protein retained at the surface was then determined. After this, another solution with a slightly higher protein concentration was injected. This procedure was repeated with steadily increasing protein concentrations, until

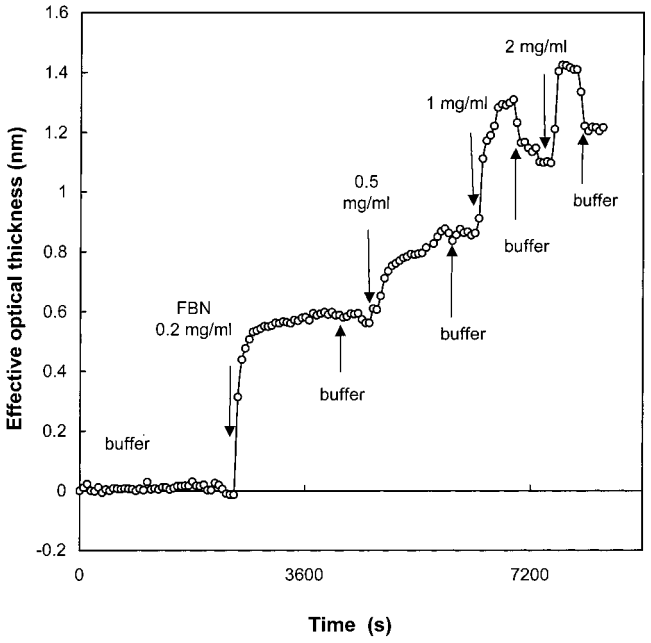

FIGURE 7: Characteristic time course for fibrinogen adsorption onto a supported DSPE monolayer measured by SPR.

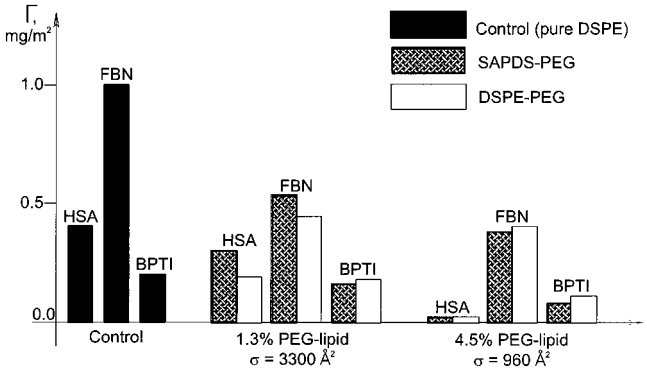

FIGURE 8: Protein adsorption both on neutral and on negatively charged lipid membranes displaying grafted PEG_{2000} at the indicated grafting densities. Fibrinogen (FBN), human serum albumin (HSA), and bovine pancreatic trypsin inhibitor (BPTI) at 0.1 mg/mL were incubated with supported lipid monolayers containing pure DSPE or mixtures of DSPE and PEG-lipid conjugates. The amount of protein adsorbed was determined by surface plasmon resonance.

there was no further change in the amount of adsorbed protein. The protein that was deposited, in units of surface density (mg/m^2), was then converted into the % coverage relative to a full protein monolayer. We assumed BPTI and HSA adsorbed in a side-on orientation (*55*). Figure 8 summarizes the results obtained with charged DSPE-PEG and with uncharged SAPDS-PEG monolayers.

There is only a small difference between BPTI adsorption on the negatively charged DSPE-PEG layers versus the neutral ones. By contrast, negatively charged DSPE-PEG monolayers adsorb slightly less of the acidic proteins, HSA and FBN, than the neutral SAPDS-PEG films do. The differences between adsorption on charged versus uncharged surfaces are, however, small. This is not surprising given the rather low surface charge densities (−3.5 mC/m^2 for 1.3 mol % and −13 mC/m^2 for 4.5 mol % DSPE-PEG) and the additional repulsion by the polymer. Also, for large proteins, which are unlikely to penetrate the polymer layer, the surface charges are screened within 1−2 debye lengths.

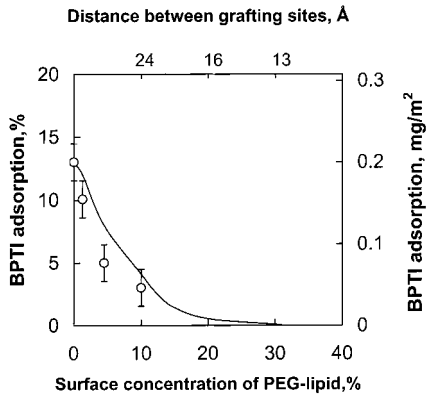

FIGURE 9: Adsorption of BPTI as a function of the SAPDS-PEG surface concentration. The solid line corresponds to the theoretically predicted dependence of the adsorption on the mole fraction of polymer−lipid in the monolayer.

The debye length under the conditions used in these studies is 13.5 Å.

Figure 9 shows the amount of BPTI adsorbed as a function of the polymer surface coverage for DSPE monolayers containing 0, 1.3, 4.5, and 10 mol % SAPDS-PEG. Note that, because both the PEG-lipid and the matrix lipid are uncharged, there is no electrostatic contribution to the adsorption. These data show that the adsorbed amount of BPTI decreases with increasing polymer concentration.

We compared this behavior with that predicted for adsorption to the underlying bilayer (primary adsorption) in the presence of grafted chains. As pointed out previously (*7*), when the protein radius is less than *s*, the distance between the grafting sites, it may penetrate the polymer layer and adsorb to the underlying surface (primary adsorption). In this case, the adsorption isotherm is determined by the equilibrium constant

$$K_{in} \approx \exp(-U_{in}/kT)$$

where U_{in} is the depth of the primary minimum at the surface

$$U_{in} \approx U_{eff}(0) \approx U_{bare}(0) + U_{brush}(0)$$

$U_{bare}(0)$ is the interaction energy with the bare lipid monolayer. It was determined from the linear regime of the protein adsorption isotherm on the bare lipid: $U_{bare}(0) = -kT \ln K_{bare}$. For BPTI, the value of K_{bare} was determined from SPR measurements with pure DSPE monolayers and was 3.6×10^3 M^{-1}. U_{bare} was, therefore, -3.37×10^{-20} J at 298 K.

$U_{brush}(0)$ is due to the osmotic penalty for inserting the protein into the brush, $U_{brush}(z) \approx P(z)\, R^3$. Using the Alexander−de Gennes model for a polymer brush, Halperin showed that $U_{in} \approx U_{bare}(0) + kT(R/\sigma^{1/2})^3$ (*7*). Then,

$$K_{in} \approx \exp-(U_{bare}(0)/kT + (R/\sigma^{1/2})^3)$$

and

$$\theta_{in} \approx K_{in}c \approx c \exp(-U_{bare}(0)/kT - (R/\sigma^{1/2})^3) \qquad (4)$$

Here c is the bulk protein concentration, and θ_{in} is the fraction of occupied primary adsorption sites. The latter variable can be converted into the coverage (% of a monolayer) by multiplying by 100.

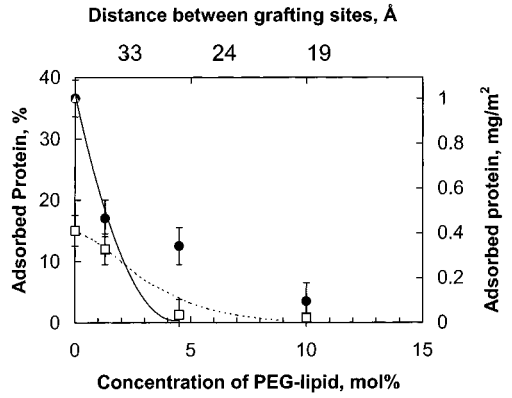

FIGURE 10: Adsorption of HSA (□) and FBN (●) as a function of the PEG-lipid surface concentration. The solid and dashed lines correspond to the theoretically predicted dependence of the protein adsorption on the surface polymer−lipid concentration.

The curve calculated with eq 4 and the experimentally determined $U_{bare}(0)$ is shown as a solid line in Figure 8. For this calculation, the BPTI molecule, which is roughly a rotational ellipsoid with radii 10.5 × 10.5 × 15 Å, was represented by a sphere of equal volume (R = 11.8 Å). As one can see, the BPTI adsorption calculated with the Halperin model is in reasonable qualitative agreement with that determined experimentally. The model also predicts that primary adsorption should be suppressed completely when the protein diameter exceeds the average distance between the grafting sites (*7*). For BPTI, this occurs at PEG surface concentrations above ~12 mol %.

The adsorption of HSA and FBN to DSPE monolayers containing 1.3, 4.5, and 10 mol % SAPDS-PEG estimated from SPR data is shown in Figure 10. Again, the adsorption decreased steadily with increasing SAPDS-PEG content in the monolayer. It approached zero for HSA at 4.5 mol % SAPDS-PEG, and FBN adsorption was suppressed at 10.0 mol % PEG-lipid. To compare this behavior with that predicted for primary protein adsorption, we calculated the amount of protein bound as a function of the polymer grafting density (eq 4). One can see that, in the case of HSA, the calculations for primary adsorption agreed qualitatively with the experimental results. With FBN, however, the model underestimates the amount of adsorbed protein, especially at higher PEG densities. This suggests that additional factors may control FBN deposition.

We considered whether the high FBN adsorption might be due to long-rang attraction between the soluble protein and the underlying membrane. Large rodlike proteins may also adsorb at the outer edge of the brush (secondary adsorption) due to, for example, the long-range van der Waals attraction between the protein and the underlying substrate. Between a surface and a rod of radius R and length H, the van der Waals potential can be approximated as

$$U_{vdW} = -\frac{AR^{1/2}H}{12\sqrt{2}L_o^{3/2}} \quad (5)$$

where L_o is the equilibrium brush thickness and A is the Hamaker constant (*56*). The Hamaker constant for protein interactions with a lipid bilayer across the hydrated polymer brush was calculated using Lifschitz theory (*56*). We assumed the refractive index (n) and the dielectric constant (ϵ) of the layer of swollen PEG chains between the protein and the membrane to be constant throughout and to depend only on the volume fraction ϕ_0 of polymer segments

$$n = \phi_0 n_{PEG} + (1 - \phi_0)\, n_{H_2O}$$

$$\epsilon = \phi_0\, \epsilon_{PEG} + (1 - \phi_0)\, \epsilon_{H_2O}$$

On the basis of the above considerations, the Hamaker constants were 6.43×10^{-21}, 6.05×10^{-21}, and 5.81×10^{-21} J for the 1.3, 4.5, and 10.0 mol % PEG-SAPDS monolayers, respectively. U_{vdW} for FBN, as given by eq 5, was only 1.07kT for 1.3 mol %, 1.01kT for 4.5 mol %, and 0.43kT for 10 mol % of SAPDS-PEG in the monolayer. Thus, although certainly present, the van der Waals attraction is too weak to be the cause of the apparent "secondary adsorption". Therefore, although it provides a good description of the adsorptions of HSA and BPTI, the model does not account for all of the interactions that control protein deposition.

In some ways, the agreement between our experimental data and the model predictions is surprising in light of the assumptions used in the scaling analysis of Halperin. The proteins are modeled as structureless spheres or cylinders. This ignores the possibility of protein deformations upon binding or heterogeneity in the protein surface composition. In addition, the description of protein interactions with polymers treats the latter as simple, structureless chains in good solvent (*7*). Such simple models do not account for bond formation between the chains and proteins. Recent reports, however, indicate that proteins bind directly to the polymer segments (*61*−*64*). Additionally, spectroscopic studies of anchored oligoethylene oxide monolayers showed that the EO segments adopt intrachain structures in water and that the different conformations interact differently with proteins (*65*). These are only a few examples, but the effects of such deviations from simple polymer behavior and their influence on PEG's biological activity have not been fully explored. Indeed, attractive interactions between the amino acid side chains of fibrinogen and the PEG segments may be responsible for the higher-than-expected FBN adsorption reported here. Nevertheless, simple polymer descriptions of protein adsorption on PEG films still allow for the formulation of simple and testable predictions. Departures from such predictions in turn facilitate determinations of the physical−chemical mechanisms responsible and may, for example, lead to establishing better design criteria for polymer-stabilized liposomes.

CONCLUSION.

These studies show that the addition of a small concentration of SAPDS-PEG in the membrane dramatically alters the interbilayer interactions. We demonstrated that the steric forces between neutral membranes comprising neutral SAPDS-PEG are well described by simple theories for grafted polymers. Further, the forces attributable to the polymers on uncharged bilayers are essentially the same as those measured between grafted PEG on negatively charged membranes. The reduction in adsorbed protein both on neutral and on charged membranes, with increasing polymer densities, also agreed with theoretical predictions. The importance of the latter results is that they demonstrate that simple theories can be used to guide the design of polymer-

coated liposomes. Our studies show that the principle difference between the neutral SAPDS-PEG and the negatively charged DSPE-PEG membranes is the electrostatic double layer force between the charged bilayers. We, therefore, attribute the differential adsorption of acidic and basic proteins on charged and neutral membranes primarily to the membrane charge. This, in turn, alters the interactions of various proteins with the bilayers, as demonstrated by surface plasmon resonance. These differences may be responsible for the differences in opsonization and phagocytosis of neutral versus charged liposomes. Alternatively, the electrostatics could alter the liposome interactions with the cell membrane directly. On the basis of these measurements alone, we cannot explicitly identify the origin of the variations in liposome uptake. However, our findings show that the differences are due to electrostatics and not to perturbations of the polymer coat.

REFERENCES

1. Harris, J. M., Ed. (1992) *Poly(ethylene glycol) Chemistry: Biotechnical and Biomedical Applications*, Plenum Press, New York.
2. Elbert, D. L., and Hubbel, J. A. (1996) *Annu. Rev. Mater. Sci. 26*, 365−370.
3. Lee, J. H., Lee, H. B., and Andrare, J. D. (1995) *Prog. Polym. Sci. 20*, 1043.
4. Milner, S., Witten, T., and Cates, M. (1988) *Macromolecules 21*, 2610−2619.
5. Alexander, S. (1977) *J. Phys. (Paris) 38*, 983−987.
6. de Gennes, P. (1981) *Macromolecules 14*, 1637−1644.
7. Halperin, A. (1999) *Langmur 15*, 2525−2533
8. Napper, D. H. (1983) *Polymeric Stabilization of Colloidal Dispersions*, Academic Press, New York.
9. Piirma, I. (1992) *Polymeric Surfactants*, Marcel Dekker, Inc., New York.
10. Wu, S. (1982) *Polymer Interfaces and Stability*, Marcel Dekker, Inc., New York.
11. Woodlie, M. C., and Lasic, D. D. (1992) *Biochim. Biophys. Acta 1113*, 171−179.
12. Kuhl, T. L., Leckband, D. E., Lasic, D. D., and Israelachvili, J. N. (1994) *Biophys. J. 66*, 1479−1488.
13. Lasic, D. D. (1993) *Liposomes: From Physics to Applications*, Elsevier, Amsterdam.
14. Lasic, D. D., and Papahadjopoulos, D. (1996) *Curr. Opin. Solid State Interface Sci. 1*, 392−409.
15. Topchieva, I. N., Efremova, N. V., Khvorov, N. V., and Magretova, N. V. (1995) *Bioconjugate Chem. 6*, 380−388.
16. Bailey, F., and Koleske, J. (1990) in *Nonionic Surfactants* (Schick, M., Ed.) p 927, Marcel Dekker, New York.
17. Woodle, M., and Lasic, D. (1992) *Biochim. Biophys. Acta 1113*, 171−178.
18. Golander, C.-G., Herron, J. N., Lim, K., Claesson, P., Stenius, P., and Andrare, J. D. (1992) in *Poly(ethylene glycol) Chemistry: Biotechnical and Biomedical Applications* (Harris, J. M., Ed.) pp 221−245, Plenum Press, New York.
19. Blume, G., and Cevc, G. (1990) *Biochim. Biophys. Acta 1029*, 91−102.
20. Gregoriadis, G., and Ryman, B. (1972) *Biochem. J. 129*, 123−133.
21. Allen, T., Hansen, C., Martin, F., Redermann, C., and Yau-Young, A. (1991) *Biochim. Biophys. Acta 1066*, 29−39.
22. Klibanov, A., Maruyama, K., Torchilin, V., and Huang, L. (1990) *FEBS Lett. 268*, 235−245.
23. Lasic, D., Martin, F., Gabizon, A., Huang, S., and Papahadjopoulos, D. (1991) *Biochim. Biophys. Acta 1070*, 187−195.
24. Allen, T., Austen, G., Chonn, A., Lin, L., and Lee, K. (1991) *Biochim. Biophys. Acta 1061*, 56−66.
25. Miller, C. R., Bondurant, B., McLean, S. D., McGovern, K. A., and O'Brien, D. F. (1998) *Biochemistry 37*, 12875−12883.
26. Israelachvili, J. N. (1973) *J. Colloid Interface Sci. 44*, 259−271.
27. Needham, D., McIntosh, T., and Lasic, D. (1992) *Biochim. Biophys. Acta 1108*, 40−47.
28. Needham, D., Hristova, K., McIntosh, T., Dewhitst, M., Wu, N., and Lasic, D. (1992) *J. Liposome Res. 2*, 411−419.
29. Kuhl, T. L., Leckband, D. E., Lasic, D. D., and Israelachvili, J. N. (1995) in *Stealth Liposomes* (Lasic, D., and Martin, F., Eds.) pp 73−91, CRC Press, Boca Raton, London, Tokyo.
30. Dolan, A., and Edwards, F. (1974) *Proc. R. Soc. London 337*, 509−516.
31. Moghimi, S. M., and Patel, H. M., Eds. (1993) *Techniques to Study the Opsonic Effect of Serum on Uptake of Liposomes by Phagocytotic Cells from Various Organs of the RES*, CRC Press, Boco Raton, FL.
32. Chonn, A., Semple, S. C., and Cullis, P. R. (1992) *J. Biol. Chem. 267*, 18 759−18 765.
33. Jeon, S. I., Lee, J. H., Andrade, J. D., and de Gennes, P. G. (1991) *J. Colloid Interface Sci. 142*, 149−158.
34. Jeon, S. I., and Andrade, J. D. (1991) *J. Colloid Interface Sci. 142*, 159−166.
35. Szleifer, I. (1997) *Biophys. J. 72*, 595−605.
36. Israelachvili, J. N., and Adams, G. E. (1978) *J. Chem. Soc., Faraday Trans. 1 74*, 975−1001.
37. Kretschmann, E., and Raether, H. (1968) *Z. Naturforsch.* Teil A *23*, 2135−2136.
38. Kretschmann, E. (1971) *Z. Phys. 241*, 313−324.
39. Lavrik, N. A., and Leckband, D. E. (2000) *Langmuir 16*, 1842−1851.
40. Spraggon, G., Everse, S. J., and Doolittle, R. F. (1997) *Nature 389*, 455−462.
41. Parkin, S., Rupp, B., and Hope, H. (1996) *Acta Crystallogr. D52*, 18−29.
42. Sugio, S., Kashima, A., Mochizuki, S., Noda, M., and Kobayashi, K. (1999) *Protein Eng. 12*, 439−446.
43. Davies, J. (1996) in *Surface Plasmon Resonance; Theory and Experimental Considerations*, CRC Press, New York.
44. Jung, L. S., Campbell C. T., Chinowsky T. M., Mar M. N., and Yee S. S. (1998) *Langmuir 14*, 5636−5648.
45. Baekmark, T. R., Wiesenthal, T., Kuhn, P., Bayerl, T. M., Nuyken, O., and Merkel, R. (1997) *Langmuir 13*, 5521−5523.
46. Majeski, J., Kuhl, T. L., Gerstenberg, M. C., Israelachvili, J. N., and Smith, G. S. (1997) *J. Phys. Chem. B 101*, 3122−3129.
47. Baekmark, T., Elender, G., Lasic, D. D., and Sackermann, E. (1995) *Langmuir 11*, 3975−3987.
48. Kuzmenka, D., and Granick, S. (1988) *Macromolecules 21*, 779−785.
49. Frey, W., Schneider, J., Ringsdorf, H., and Sackmann, E. (1987) *Macromolecules 20*, 1312−1321.
50. Marra, J., and Israelachvili, J. (1985) *Biochemistry 24*, 4608−4618.
51. Kenworthy, A. K., Hristova, K., Needham, D., and McIntosh, T. J. (1995) *Biophys. J. 68*, 1921−1936.
52. Derjaguin, B. (1934) *Kolloid Z. 69*, 155−172.
53. Kuhl, T. L., Majeski, J., Wong, J. Y., Steinberg, S., Leckband, D. E., Israelachvili, J. N., and G. S., S. (1998) *Biophys. J. 75*, 2352−2362.
54. Bianco-Peled, H., Dori, Y., Schneider, J., Tirrell, M., Sung, L.-P., and Satija, S. (1999) *Langmuir* (in press).
55. McPherson, T., Kidane, A., Szeleifer, I., and Park, K. (1998) *Langmuir 14*, 176−186.
56. Israelachvili, J. N. (1991) *Intramolecular and Surface forces*, Academic Press, London.
57. Hamiaux, C., Prange, T., Ries-Kautt, M., Ducruix, A., Lafont, S., Astier, J. P., and Veesler, S. (1999) *Acta Crystallogr. D Biol. Crystallogr. 55*, 103−113.
58. Asami, O., Nakamura, T., Mura, T., and Ichihara, A. (1984) *J. Biochem. (Tokyo) 95*(2), 299−309.
59. Peters, T., Jr. (1975) in *The Plasma Proteins − Structure, Function and Genetic Control* (Putnam, F., Ed.), Vol. 1, pp 146−157, Academic Press, New York.
60. Mrksich, M., Sigal, G. B., and Whitesides, G. M. (1995) *Langmuir 11*, 4383−4385.

61. Sheth, S. R., and Leckband, D. (1997) *Proc. Natl. Acad. Sci. U.S.A. 94*, 8399−8405.
62. Abbott, N. L., Blankschtein, D., and Hatton, T. A. (1992) *Macromolecules 25*, 3932−3941.
63. Cleland, J. L., Builder, S. E., Swartz, J. R., Winkler, M., Chang, J. Y., and Wang, D. (1992) *Biotechnology 10*, 1013−1019.
64. Sheth, S. R., and Leckband, D. Unpublished observations.
65. Harder, P., Grunze, M., Dahint, R., Whitesides, G. M., and Laibinis, P. E. (1998) *J. Phys. Chem. 102*, 426−436.

BI992095R